International Journal of Research in Applied Sciences & Engineering (IJRASE)
Online ISSN: 2456-2920; Volume 1, Issue 1; January 2016 pp. 72-81

Nano Phosphor MgO: Tb^{3+}: Propellant Chemistry Route and Photoluminescence Properties for White Light Discharge under NUV Excitation

P.B. Devaraja[1], Ratnam Paskaramoorthy[2], S.C. Prashantha[3*], H.P. Nagaswarupa[3], S.C. Sharma[4], H. Nagabhushana[1], K.S. Anantharaju[5]

[1]*Prof. C.N.R. Rao Centre for Advanced Materials, Tumkur University, Tumkur 572 103, India*
[2]*Department of Mechanical Engineering, University of the Witwatersrand Johannesburg, South Africa*
[3]*Research Centre, Department of Science, EWIT, Bangalore-560 091, India*
[4] *Professor of Eminence and Director, Department of Mechanical Engineering, DSCE, Provost, Dayananda Sagar University, Bangalore- 560078, India.*
[5]*Department of Chemistry, Dayananda Sagar College of Engineering, Kumaraswamy Layout, Bangalore 560078, India*
[*]*scphysics@gmail.com*

Abstract: **A low temperature solution combustion technique (400 ^{o}C) is used in the preparation of Tb^{3+} doped (1-9 mol %) MgO nanoparticles with glycine as a fuel and magnesium nitrate as precursor. The XRD patterns of the powder discovered cubic structure with average crystallite size of 5-10 nm. A porous structure in Scanning electron microscopy showed that the crystallites were agglomerated. The MgO luminescence characteristics due to the effect of Tb^{3+} cations were studied and the results were discussed in detail. The excitation nearby ultra violet (331 nm) phosphor exhibits bright green emission. Because of dipole and quadropole interactions the emission peaks characteristics at 436, 450 nm in blue region were $^5D_3 \rightarrow {}^7F_j$ (j= 4, 3), the peaks at 488, 543 in green region, 598 and 630 nm in red region were corresponding to Tb^{3+} transitions. In white region the resultant CIE chromaticity co-ordinates make the phosphor which is highly useful for display applications as well as white light-emitting diodes.**

Keywords: **MgO: $Tb3^{+}$; Nanophosphor; Photoluminescence; WLEDs; CIE.**

1. INTRODUCTION

In comparison with the predictable illumination apparatus the white light emitting diodes showed numerous benefits like low power consumption, great luminous effectiveness, environmental protection and preservation [1–2]. WLEDs, can be fabricated in two different methods namely, nearby-ultraviolet (NUV) chip plus tricolour (green, red, and blue) phosphors and blue chip plus yellow phosphor. WLEDs made-up with NUV chips and tricolour phosphors developed colour interpretation indicator that of current profitable WLED's because of emission is through only phosphors material [3-4].

Usually using a appropriate anchor material with an additional activator the phosphors are made. Generally, anchor materials having superior mechanical, optical and thermal properties are used. Usually nitrides, oxides, sulfides, and silicates are used as host materials [5]. Trivalent Eu, Tb, Dy and Tm ions which are known as rare earth activators exhibit a exceptional optical performance when doped in to anchor material. These ions luminescence properties were attributed to electronic transition which occur inside the partly filled lanthanide series of energy shell 4f [6]. Emission properties are remarkable in the narrow-band of the trivalent rare earth ions which are employed in the advance of proficient phosphors [7]. As activators trivalent Tb ions are utilized for better and capable blue and green discharge. This emanates from transitions of $^5D_3$ and $^5D_4$ excited states to the $^7F_{J\ (J=\ 0\ -\ 6)}$ ground state of trivalent Tb ions. When energized by UV energy, trivalent Tb ions ($^4F_8$) lifted to upper $^4F_7$,$^5D_1$ level and give afterwards to the $^5D_3$ or $^5D_4$ excited states [8-9].

An insulating oxide having wide band gap (~ 6.0 eV) is Magnesium oxide (MgO). It has high-melting point (~2830^{o}C), high secondary electron emission yield and low heat capacity [10, 11] and also been used in applications of optoelectronic such as plasma display panels [12], photo electrochemical solar cells, gate-controlled devices, metal oxide semiconductor and extraordinary-temperature superconductor [13–15]. Freshly, MgO particles have gained greatest attention due to stimulating properties like great surface-to-volume ratio, great catalytic activity, and low-temperature sintering with durable microwave absorption ability. Addition to these type properties it can also be used as electrochemical biosensors [16], as additives for refractories bactericides [17], and catalyst [18]. MgO has proved to be the excellent luminescent material as its synthesis is possible at low temperature and has high stability, high luminescence efficiency and inexpensive. In the past few years, a number of

MgO doped red and green emitting nanophosphors were reported for its extensive use in WLEDs applications [19].

In this paper, an MgO: Tb^{3+} nanocompounds based green phosphor was synthesized by solution combustion method using glycine as a fuel which is self-propagating. By powder X-ray diffraction (PXRD), Scanning electron microscopy (SEM), Fourier transform infrared spectroscopy (FTIR), and transmission electron microscopy (TEM) the final products were well characterized and its photoluminescent properties were investigated. In the present work, photoluminescence properties of different concentrations of Tb^{3+} ions in MgO host material are discussed in detail.

2. EXPERIMENTAL

2.1. Synthesis

The solution combustion method a series of phosphor nanopowders *i.e*. MgO: Tb^{3+} (1 - 9 mol %) were prepared. The stoichiometric composition metal nitrates such as nitrate of magnesium [$Mg(NO_3)_2$ (Sigma-Aldrich)], nitrate of terbium [$Tb(NO_3)_3$ (analar)] are used as oxidizer and glycine [NH_2CH_2COOH (analar)] as fuel. The molar ratio of 1:1.75 nitrates of metal (oxidizers) to glycine (fuel) was considered. Initially the materials were dissolved in distilled water and in the range 1-9 mol% Tb^{3+}concentration was mixed in relation to Mg content. Using magnetic stirrer the materials in a Petri dish with minimum quantity of double distilled water was mixed thoroughly and was then introduced into a pre heated muffle furnace to maintain temperature at ~ 400 ^oC. The solution undergone the dehydration, and was finally decomposed with the gases evolved. With a flame of smoldering type forming foam ruptured the mixture which was frothed and swelled. The combustion synthesis will be finished in very short period. The voluminous foamy combustion product was grinded well and used for characterization and studies.

2.2. Characterization

PXRD of Powder characterized using X-ray diffractometer (Shimadzu). Morphology of the samples was characterized using Hitachi table top Scanning electron microscopy. The product surface morphology was examined and also transmission electron microscopy (TEM). The functional group studies were performed by FTIR. Spectrofluorimeter Photoluminescence studies were made at Room Temperature and as excitation source xenon 450 W was used. For spectral analysis the Fluor Essence™ software was used.

3. RESULTS AND ANALYSIS

Undoped and trivalent Tb (1-9 mol %) doped MgO PXRD patterns of as-formed samples without any further calcinations (Fig. 1). All well indexed diffraction peaks in 2θ scale, 35.57 (1 1 1), 42.59 (2 0 0), 62 (2 2 0), 74.28 (3 1 1), 78.34 (2 2 2) show pure single cubic phase, that matches (JCPDS 4 – 0829) by space group $Fm\bar{3}m$ (225) [20]. Lattice parameter and unit cell volume is valued for plane (200) expending relations (1) & (2) is originate about 4.3 Å and 79.507 $Å^3$ respectively.

$$2d\sin\theta = n\lambda \quad \ldots. \quad (1)$$

$$d_{hkl} = \frac{a}{\sqrt{\left(h^2+k^2+l^2\right)}} \quad \ldots. \quad (2)$$

It was clear from the PXRD analysis, crystal arrangement doesn't inspire with the insertion of trivalent Tb ion, this is because, the alteration in ionic radii amongst substituted rare-earth and Mg ion (the ionic radii of R_{Tb}^{3+} = 0.0923 nm and R_{Mg}^{2+} = 0.072 nm) definitely adapted the lattice parameters. The normal crystallite dimensions (D) projected from line expansion in X-ray information by means of Scherer's equation [21]

$$D = \frac{k\lambda}{\beta\cos\theta} \quad \ldots. \quad (3)$$

[Where, 'K'; spherical symmetry constant usually considered as 0.89 – 0.9 for polycrystalline almost spherical samples, 'λ'; wavelength of CuKα radiations of X-rays, 'β'; full width half maxima (FWHM)]. D value was found in the range 5-10 nm. Expansion of the unit cell is caused by Tb^{3+} ions which are doped into MgO matrix also results in tensile stress, due to which the peaks are shifted towards higher angle side [22]. The attendance of micro strain in nanophosphors gives raise to the peak change and line expansion profiles.

Further, strain present is calculated by W-H plots for MgO: Tb^{3+} (1-9 mol %) nanoparticles which are manufactured by combustion synthesis using equation (4)

$$\frac{\beta\cos\theta}{\lambda} = \frac{1}{\varepsilon} + \frac{\eta\sin\theta}{\lambda} \quad \ldots. \quad (4)$$

where 'ε' is the strain associated with the nanoparticles [23]. A straight line between '4 sinθ' (x-axis) and 'β cosθ' (y-axis) is represented by the above equation as exposed in Fig.2 (a). To study size - strain parameters the Nelson-Riley method is likewise used as shown in Fig.2 (b). In this method, by a Lorentzian function crystallite size is described by Gaussian function [24].

$$\left(d_{hkl}\,\beta_{hkl}\cos\theta\right)^2 = \frac{k\lambda}{D}\left(d_{hkl}\,\beta_{hkl}\cos\theta\right) + \left(\frac{\varepsilon}{2}\right)^2 \quad \ldots(5)$$

Where k is constant which depends on their morphology; alike to W-H plots, factor $(d_{hkl}\,\beta_{hkl}\cos\theta)^2$ is plotted with respect to $(d_{hkl}\,\beta_{hkl}\cos\theta)$ for entire alignment peaks of MgO. Systematic crystallite structure computed by Scherrer's method, W-H plan & size-strain plan are almost same, decreases with Tb^{3+} concentration & values are lesser equated to undoped material; however the strain values are originate to intensification with increase in trivalent Tb concentration. Being non-stochiometric oxygen and grain boundary defects the increase in strain was mainly attributed [25]. the radii mismatch of Tb and Magnesium leads to additional oxygen vacancies which are made in lattice introduces the defects were explained by defect reaction equation in subsequent section, as a outcome this additional lattice strain were likely expected in Tb doped nanophosphors [26].

Samples PXRD data is validated statistically for following reasons firstly to obtain the exact lattice parameters, by using *FULLPROF* software [27] Rietveld refinement analysis (Fig. 3) was done, assuming $Fm\overline{3}m$*(225)*. To fit the various parameters Pseudo-voigt function was utilized two asymmetric factors and one global thermal factor). The lattice parameters and refined structural parameters were given in Tables 1 and 2. The refined and observed PXRD pattern holds good agreement in fitting parameters (R_p, R_{wp} and χ^2) for the cubic phase.

The ionic radii amongst doped and replaced ions acceptable percentage difference necessity not crossed 30%. Based on the formula the radius % difference (Dr) calculations amongst trivalent Tb doped and replaced Mg^{2+} in Tb doped MgO is considered [28, 29]:

$$D_r = \frac{R_m(CN) - R_d(CN)}{R_m(CN)} \qquad \ldots. \quad (6)$$

The SEM surface features texture and topography of the nanophosphors were characterized. It is evidently witnessed from the SEM photos as seen in Fig. 4 (a-d) powders are extremely permeable in nature, agglomerated asymmetrical particle shape, cracks, big voids and pores. During combustion process the discharge of huge quantity of gases occurrence is the main reason [30, 31]. The nanoparticles crystalline characteristics were carried out using TEM. Fig. 5 (a-d) demonstrates the TEM photos of pristine MgO nanoparticles. The irregularly shaped and highly dispersed particles are observed. The ring pattern obtained by Selected Area Electron Diffraction (SAED) figure is indication for the polycrystalline performance of synthesized nanoparticles and the results were detailed in Table 3. Further, by high resolution TEM (HRTEM) a distinct lattice fringes obtained a pattern revealing the information of highly crystalline pure MgO nanophosphor [32]. The 0.253 nm is the spacing between adjacent nanoparticles lattice fringes, actual near to that of 0.246 nm for MgO. The presence of Mg and O is clear by the EDX result where the Mg and O peaks appeared without any other characteristic peaks. However, for TEM analysis the peaks corresponding to Cu due to carbon coated copper grid are used. Hence, to suggest the results are definite evidence of that the sample do not contain any other element and are free from impurities.

MgO: Tb^{3+} samples Fourier transform infrared (FTIR) spectra were shown in Fig. 6. The strong signature bond at 415 cm^{-1} is accompanying with the distinguishing vibrational manner of symmetric MgO_6 octahedral sites. Additional, the peaks at 550-850 cm^{-1} (γ_1) are higher frequency stretching of MgO and 410-450 cm^{-1} (γ_2) is inferior frequency stretching. Mg-O-Mg interactions peak at 860 cm^{-1} is attributed. 1300-1800 cm^{-1} is the absorption range of related hydroxyl group of molecular water at 1643 cm^{-1}, NH_3 at 1480 cm^{-1} and it was due to C=O stretching mode. Due to absorption of atmospheric CO_2 the peak at ~2400 cm^{-1} arises on the metallic cations. Also, the presence of hydroxyl groups is indicated by the absorption at ~3500 cm^{-1} (O-H mode), the spectrum were not recorded in situ, which is probably due to the fact that the some water re-adsorption at ambient atmosphere [33,34].

The Tb^{3+} doped MgO nanophosphor excitation spectrum recorded with emission centered 544 nm was found inset Fig. 7. At 285 nm (short ultraviolet region) the excitation peak centered was charge transfer band (CTB) of Tb^{3+}-O^{2-}. At 331 nm the excitation greatest was found. The optical assimilation moves comparing to these wavelengths are inside of the 4f shell.

Due to f-f transitions of Tb^{3+} ions a series of sharp lines were centered at 318, 331, 341, 351, 369, 377 and 399 nm, labeled to spin-allowed (SA) 4f →5d bands within 300 - 330 nm, and spin-forbidden (SF) 4f→5d bands within 330–400 nm [28, 35].Transition from $^7F_6$ ground state to excited states of $^4F_8$ configuration is related to lengthier wavelengths. Greatest penetrating lines with greatest at 369 and 377 nm are allocated to the $^7F_6$→ ($^5G_6$, $^5G_5$, $^5L_9$) and $^7F_6$→ ($^5D_3$, $^5L_{10}$) on the energy level foundation for Tb^{3+} ion [36-38]. With near UV radiation these excitation peaks inform that MgO: Tb^{3+} phosphors can be efficiently excited. It is interesting to note that GaN-based LED chips can be used as an excitation source for the present phosphor [39, 40].

Fig. 7 shows at 331 nm emanation spectra of Tb doped MgO (1-9 mol %) is excited. In general, due to transitions the emanation of Tb^{3+} ions occurs at $^5D_3$ and $^5D_4$ excited states to the ^7F_J ground states. In two groups the emission spectrum lines are separated, $^5D_3$ → ^7F_J belongs to blue emission group below 480 nm and green emission from $^5D_4$→^7F_J (J=6, 5, 4

and 3) over 480 nm. Emission peaks at 436, 450 nm (blue emissions) resultant to $^5D_3 \rightarrow {}^7F_4$, $^5D_3 \rightarrow {}^7F_3$ transitions & 488, 543, 598, 630 nm (green emissions) to the electronic transitions which are attributed at $^5D_4 \rightarrow {}^7F_6$, $^5D_4 \rightarrow {}^7F_5$, $^5D_4 \rightarrow {}^7F_4$ and $^5D_4 \rightarrow {}^7F_3$, respectively [41-44].

On the basis of the schematic diagram the luminescence mechanism was explained for energy levels as shown in Fig. 8. Transition of 4f–5d under the NUV-excitation (331 nm), Tb^{3+} ions are excited. In conduction band (CB) electrons are reassigned to 5d positions and leaving holes behind. Then complete valence band (VB) holes are moved. Some electrons, in 5d positions of Tb^{3+} relocated and tranquil to $^5D_3$ level subsequent of distinguishing emission of Tb^{3+} as deliberated [45]. At the corner Mg molecules are contemporary in the cube and corresponding by 8 comparable neighbor oxygen atoms. The point bunch in lattice is symmetry of Mg locales in MgO cubic arrangement is in a perfect world D_{2d} and Mg site has reversal symmetry. The host is doped with RE^{3+} ion, they likely possess these locales. Notwithstanding, the PL results demonstrate that RE^{3+} ion in MgO is chiefly arranged more at the low symmetry locales. The RE_2O_3 overabundance sum will probably dwell on either surface or nanocrystals grain limits to get ideal strain release.

In present research work the rare earth oxide even at 9 mol % do not have diffraction peaks shows Tb^{3+} ions enters the host cross section and supplant Mg ion situated on base of nano crystals in view of the porosity of MgO [46]. Accompanying way the defect reaction comparison can be illustrated by using following equation 7.

$$(1-x)MgO+0.5(Tb_2O_3)_x = xTb_{oc}^{\bullet} + 0.5(V_0^{\bullet\bullet})_x + (1-x)Mg_{Mg}^{x} + (2-0.5x)O_0^{x} \quad (7)$$

where 'Tb_{oc}' is Tb occupancy to the normally occupied sites of 'Mg^{2+}' were replacement by 'Tb', '$V_0^{\bullet\bullet}$' is 'O^{2-}' vacancy, 'Mg_{Mg}^{x}' signifies the rest of Mg in the lattice of pristine ', O_0^{x} ' oxygen in MgO lattice [47].

Specifically, at 543 nm emission peak compares to $^5D4 \rightarrow {}^7F_5$ & happens *via* forced electric-dipole (FED) is permitted without a reverse focus the Tb^{3+} particle involves a site. At 543 nm Transition is centered and the normal for green emission affirms the energy transfer from MgO to Tb^{3+} [48]. Both odd - even equality state intensities depend upon and J–Jo blending inside of the 4f- electron state complex, whereas the $^5D_4 \rightarrow {}_7F_6$ at 488 nm is the magnetic-dipole move which has no electric dipole commitment. At specific intrigue these two emissions (488 and 543 nm) are spoken to really by the neighborhood situation of the Tb^{3+} particles. Emission peaks of relative PL intensity rely on upon the symmetry of the Tb^{3+} activator ions, & it portrayed as far as Judd–Ofelt hypothesis [49]. As dopant concentration increases, the emission intensity increases up to 3 mol % of Tb^{3+} $^5D_4 \rightarrow {}^7F_5$ and transition dominates. The increase in distortion may be attributed to the local field everywhere the Tb^{3+} particles [44]. Furthermore, the lattice there is charge imbalance because of trivalent Tb^{3+}doping.

The relative intensity Tb^{3+} relies on upon the doping concentration of Tb^{3+} in MgO phosphor was demonstrated The emanation transition centered at $^5D_4 \rightarrow {}^7F_5$ (543 nm) demonstrates improved emission with increase in the concentration of Tb ion. At the point when the Tb^{3+} particles fixation expands over 3 mol %, PL discharge force starts to diminishing demonstrates concentration quenching (Inset Fig. 9a). On the premise of taking after two aspects the concentration quenching may be clarified: (i) the excitation movement because of when the doping concentration is expanded the resonance between the activators gets upgraded, and along these lines the excitation energy reaches quenching center; (ii) activators were combined or coagulated & distorted to quenching concentration. Non-radiatively energy exchanged by the energy reabsorption or multipole-multipole connection [50]. Likewise, increment in Tb^{3+} fixation can bring about low concentration procedures in close Tb^{3+}–Tb^{3+} sets, the quenching of Tb^{3+} luminescence regularly happens at very low Tb concentration. Tb^{3+} particles would enter into magnesium substitution positions, the majority may be ingested at the surface of the nano-crystalline MgO, which offers a great deal additional open door for cross-relaxation procedures and comparable outcome were accounted by F. Gu *et al* in MgO:Dy at 1.5 % Dy focus [51].

$$A_{21} = \frac{\oint I_2 \lambda_{543}}{\oint I_1 \lambda_{487}} \qquad -----(8)$$

With increase of Tb^{3+} ions the values of A_{21} decrease. However, Tb3+ doping will introduce lattice defects it is reasonable to believe that which will lessen the symmetry quality of the neighborhood environment of Mg^{2+} locales. Thus, with the increment of doped Tb3+ fixation the symmetry proportion of MgO: Tb^{3+} diminishes. The Rc, critical transfer distance for energy transmission were determined with Blasse [52]

$$R_c \approx 2\left[\frac{3V}{4\pi X_c N}\right]^{1/3} \qquad ------(9)$$

The Rc in MgO: Tb^{3+} is computed to 10.59 Å. For this situation, Tb^{3+}– Tb^{3+} separation bigger than 5 Å the trade and re-absorption connection gets to be incapable. Accordingly,

the vitality exchange between Tb^{3+} particles in MgO phosphor ought to happen just by electric multipolar connection. Van Uitert report [53], convergence of Tb^{3+} is more noteworthy over the basic one, outflow force of multipolar-association for each activator particle can be resolved from the mathematical statement [54].

$$\frac{I}{x} = k\left[1 + \beta(x)^{Q/3}\right]^{-1} \quad -----(10)$$

Fig. 9(b) demonstrates log (I/x) v/s log (x) as concentration dependence curve. Reliance of log (I/x) on log x is direct, and the incline is ~ - 1.3275. Estimation of "Q" can be figured as 8.3605, which is very near to 8.

Commission International De I-Eclairage (CIE) chromaticity co-ordinates for trivalent Tb doped MgO (3 mol %) as a component of Tb^{3+} fixation for color was delineated by PL. The CIE directions figured from PL spectra (x=0.295, y=0.247) are appeared in Fig. 10 [55]. It was noted that the CIE co-ordinates of Tb^{3+} incorporated MgO: Tb^{3+} was near the National Television System Committee (NTSC) regular qualities, they drop near white area of chromaticity outline and their comparing area was stamped with star in white location. Coordinated color temperature (CCT) assessed by Planckian locus, which is just a little partition of (x, y) chromaticity chart and there exist numerous working focuses outside Planckian locus. CCT is ascertained by changing (x, y) directions of light source to (U', V') by utilizing taking after mathematical statements, and by deciding the temperature of the nearest purpose of Planckian locus to light source on the (U', V') uniform chromaticity chart (Fig. 11) [56].

$$U' = \frac{4x}{-2x + 12y + 3} \quad (11)$$

$$V' = \frac{9y}{-2x + 12y + 3} \quad .... \quad (12)$$

The CCT originate from 11060 K by using U′=0.2196, V′=0.4137. Hence, current phosphor shows the potentiality to use in white LEDs and for the manufacture of unnatural white light in solid state display applications which is nearly same as that of expected white light due to its enhanced spectral overlap.

4. CONCLUSIONS

Tb^{3+}- doped MgO nanophosphors are synthesized via facile route. MgO phosphors diffraction patterns shows a single cubic phase. The average crystallite size calculated is in the range of 5-10 nm with agglomeration. In the range of 40-50 nm the average particle size was found. At 543 nm, the emanation spectra of MgO: Tb^{3+} is interrelated towards $^5D_4 \rightarrow {}^7F_J$ transitions of trivalent Tb ion, the greatest strong emission of Tb^{3+} is recorded for ($^5D_4 \rightarrow {}^7F_5$) transition. The estimated CIE chromaticity and the excellent white emission properties co-ordinates (x=0.295, y=0.247) very close to NTSC standard value of white emission of synthesized phosphor. Hence, the promising material is optimized MgO: Tb^{3+} nanophosphors which can be widely used in optical display systems.

REFERENCES

[1] Fu Yanga, Z. Yang, Q. Yu, Y ufeng Liu, XuLi, Fachun Lu, Spectr. Acta Part A: Molecu. Biome. Spectra. **105** (2013) 626–631.

[2] G. M. Cai , J. J. Fan , H. K. Li , Z. Zhao, L. M. Su , Z. P. Jin,, J. Alloys Compd. **562** (2013) 182–186.

[3] L. S. Zhao, J. Liu, Z. C. Wu, S. P. Kuang, Spectr. Acta Part A: Molec. Biom. Spectr. **87** (2012) 228–231.

[4] Ru. Yuan Yang , H. Lin Lai Graduate, J. Lumin. **145** (2014) 49–54.

[5] H. A. Ahmed, O. M. Ntwaeaborw, R. E. Kroon, J. Lumine. **135** (2013) 15–19.

[6] Xiaohua Liu, Wendou Xiang, Fengming Chen, Zhengfa Hu, Wei Zhang,Mater Rese Bull. **48** (2013) 281–285.

[7] JiayueSunn, Junhui Zeng, Yining Sun, Jicheng Zhu, Haiyan Du, Ceram Intern. **39** (2013) 1097–1102.

[8] E. Pavitra, Jae Su Yu, Cera Intern . **39** (2013) 1029–1036.

[9] Z. Kotan, M. Ayvacikli, Y. Karabulut, J. Garcia-Guinea, L. Tormo, A. Canimoglu, T. Karali, N. Can, J. Alloys Compd**. 581** (2013) 101–108.

[10] J. Zhang, L.D. Zhang, Chemical Physics Letters. **363** (2002) 293–297.

[11] S. Azzaza, M. El-Hilo, S. Narayanan, J. Judith Vijaya, N. Mamouni, A. Benyoussef, A. El Kenz, M. Bououdina, MatrChem Phys. **143** (2014) 1500-1507.

[12] Mingji Li, Xiufeng Wang, Hongji Li, Hairong Di, Xiaoguo Wu, Changri Fang, Baohe Yang,Appl Surf Scie. **274** (2013) 188–194.

[13] Y. B. Li, Y. Bando, T. Sato, Chem. Phy. Lett. **359** (2002) 141–145.

[14] K. Hayashi, S. Matsuishi, T. Kamiya, M. Hirano, H. Hosono, Nature. 419 (2002) 462–465.

[15] Ru Yuan Yang, Yu-Ming Peng, Hsuan-Lin Lai, Cheng-Jye Chu, BrigetteChiou, Yan-Kuin Su, Optical Materials. **35** (2013) 1719–1723.

[16] J. Zhao, L. Qin, Y. Hao, Q. Guo, F. Mu, Z. Yan, Mikrochimica. Acta.. **178** (2012) 439 –445.

[17] M. A. Shah, F. M. Al-Marzouki, I. J. Biom Nanos Nanotech. **1** (2010) 10–16.

[18] N. Sutradha, A. Sinhamahapatr, B. Roy, H. C. Bajaj, I. Mukhopadhyay, A. B. Panda, Mater. Res. Bull. **46** (2011) 2163–2167.

[19] P. B. Devaraja, D. N. Avadhani, S. C. Prashantha, H. Nagabhushana, S. C. Sharma, B. M. Nagabhushana, H. P.

Nagaswarupa, H. B. Premkumar. Spectra. Acta Part A.: Molecu. Biome. Spectra. **121** (2014) 46–52.

[20] F. Gu, C. Li, H. Jiang, J. Crys. Growth., **289** (2006) 400 - 404.

[21] S. C. Prashantha, B. N. Lakshminarasappa, F. Singh. J. Lumine. **132** (2012) 3093-3097.

[22] A. Reddy, M. Kokila, H. Nagabhushana, S. C. Sharma, J. L. Rao, C. Shivakumara, B. M. Nagabhushana, R. P. S. Chakradar, Mater. Chemi. Phys. **133** (2012) 876-883.

[23] G. K. Williamson, W. H. Hall, Acta. Metall. **1** (1953) 22-31.

[24] M. Tagliente, M. Massaro, Instrume. Method Phy. Res. B. 266 (2008) 1055-1061.

[25] P. Klug, L. Alexander, In: X-ray Diffraction Procedure, Wiley, New York, 1954.

[26] J. Malleshappa, H.Nagabhushana, S. C. Sharma, D. V. Sunitha, N. Dhananjaya, C. Shivakumara, B. M. Nagabhushana, J. Alloys Compd. **590** (2014) 131-139.

[27] R.W.G. Wyckoff, Crystal Structures, Interscience, New York, 1964 (pp. 4–5).

[28] Ramachandra Naik, S.C. Prashantha, H. Nagabhushana, H.P. Nagaswarupa, K.S. Anantharaju, S.C. Sharma, B.M. Nagabhushana, H.B. Premkumar, K.M. Girish, J. Alloy Compd. **617** (2014) 69-75.

[29] Y. S. Vidya, K. Gurushantha, H. Nagabhushana, S. C. Sharma, K. S. Anantharaju, C. Shivakumara, D. Suresh, H. P. Nagaswarupa, S. C. Prashantha, M. R. Anilkumar J. Alloys Compd. **622** (2015) 86-96.

[30] P. B. Devaraja, D.N. Avadhani, S. C. Prashantha, H. Nagabhushana, S. C. Sharma, B. M. Nagabhushana, H. P. Nagaswarupa, Spectra. Acta Part A: Molec. Biom. Spectr. 118 (2014) 847-851.

[31] D. Yong Chung, E. Lee, J. Alloys Compd. **374** (2004) 69–73.

[32] M. Shivram, S. C. Prashantha, H. Nagabhushana, S. C. Sharma, K. Thyagarajan, R. Harikrishna, B. M. Nagabhushana, Spectro. Acta Part A: Molec. Biom. Spectr. 120(2014) 395–400.

[33] T. Selvamani, T. Yagyu, S. Kawasaki, I. Mukhopadhyay, Catal. Communi., **11** (2010) 537-541.

[34] S. M. Borghei, S. Kamali, M. H. Shakib, A. Bazrafshan, M. J. Ghoranneviss, J. Fusi. Ener. 30 (2011) 433-436.

[35] B.M. Manohara, H. Nagabhushana, D. V. Sunitha, K. Thyagarajan, B. Daruka Prasad, S.C. Sharma, B.M. Nagabhushana, R.P.S. Chakradhar, J. Alloy Compd. **592** (2014) 319-327.

[36] A. da Silva, M. Cebim, M. Davolos, J. Lumine. **128** (2008) 1165-1168.

[37] F.Angiuli, E.Cavalli, Al.Belletti, J. Solid State Chemi. **192** (2012) 289– 295.

[38] E. Pavitra, Jae Su Yun, Ceram Interl **39** (2013) 1029–1036.

[39] I. Akasaki, H. Amano, K. Itoh, N. Koide, K. Manabe, Insti. Phys. Confe. Seri. **129** (1992) 851.

[40] I. Akasaki, H. Amano, Jpn. J. Appli. Physi. **36** (1997) 5393.

[41] J. Young Park, H.Chae Jung, G.S. Rama Raju, B. Moon, J.Hyun Jeong, J.g Hwan Kim, J. Lumine. **130** (2010) 478–482.

[42] X. Ju, X. Li, W. Li, C. Tao, J. Yang, Matr Lett., **77** (2012) 35–37.

[43] A. Dhahri, K. HorchaniNaifer, A. Benedetti, F. Enrichi, M. Férid, P. Riello, Optic Matr. **35**(2013) 1184–1188.

[44] Mengjiao Xu, Luxiang Wang, DianzengJia, Fuhe Le, J. Lumin. 158 (2015) 125-129.

[45] YahongJin, Y. Hu, Li Chen, Xiaojuan Wang, GuifangJu, Z. Mu, J. Lumine. **138** (2013) 83 –88.

[46] P. B. Devaraja, D. N. Avadhani, H. Nagabhushana, S. C. Prashantha, S. C. Sharma, B. M. Nagabhushana, H. P. Nagaswarupa, and B. Daruka Prasad, Mate. Chart. **97** (2014) 27-36.

[47] S. Shi, M. Hossu, R. Hall, W. Chen, J. Mater Chem. **22** (2012) 23461-23467.

[48] Hongmei Yang, Jianxin Shi, Menglian Gong, K. W. Cheah, J. Lumin. **118** (2006) 257–264.

[49] B. R. Judd, Phys. Rev. **127** (1962) 750-761.

[50] H. B. Premkumar, H. Nagabhushana, S. C. Sharma, S. C. Prashantha, H. P. Nagaswarupa, B. M. Nagabhushana, R. P. S. Chakradhar, J. Alloys Compd. **601** (2014) 75-84.

[51] F. Gu, S.F. Wang, M.K. Lü, W.G. Zou, G.J. Zhou, D. Xu, D.R. Yuan, J. Cryst. Growth. **260** (2004) 507–510.

[52] G. Blasse, J. Solid State Chemi. 62 (1986) 207-211.

[53] L.G. Van Uitert, J. Electrochem. Soc. **114** (1967) 1048-1053.

[54] X. Zhang, H. JinSeo, J. Alloys Compd. **503** (2010) L14–L17.

[55] M.A. Mickens, Z. Assefa, J. Lumin. **145** (2014) 498–506.

[56] Schanda, János; Danyi, M, Color Research & Application. **2**(1977) 161–163.

TABLES

TABLE 1: Crystallite size of trivalent Tb doped MgO nanophosphor

(Tb^{3+} mol %)	Crystallite size in nm	
	Scherrer's	W-H
undoped	6.82	8.89
1	6.60	8.83
3	6.23	8.58
5	5.64	8.30
7	5.49	8.10
9	5.38	7.80

TABLE 2: Rietveld Refinement of the MgO compound doped with different Tb^{3+} concentration.

Compounds	**MgO: 1 mol% Tb^{3+}**	**MgO: 3 mol% Tb^{3+}**	**MgO: 5 mol% Tb^{3+}**	MgO: 7 mol% Tb3+	**MgO: 9 mol% Tb^{3+}**
Crystal system	Cubic	Cubic	Cubic	Cubic	Cubic
Space group	F m -3 m	F m -3 m	F m -3 m	F m -3 m	F m -3 m
Hall Symbol	-F 4 2 3	-F 4 2 3	-F 4 2 3	-F 4 2 3	-F 4 2 3
Lattice parameters (Å)					
a = b = c	4.2321	4.2321	4.2321	4.2407	4.2321
Unit cell volume ($Å^3$)	75.80	75.80	75.80	76.26	75.79
Atomic Coordinates					
Mg					
x	0.0000	0.0000	0.0000	0.0000	0.0000
y	0.0000	0.0000	0.0000	0.0000	0.0000
z	0.0000	0.0000	0.0000	0.0000	0.0000
Occupancy	0.5400	0.5383	0.4121	0.3930	0.3736
Tb^{3+}					
x	0.0000	0.0000	0.0000	0.0000	0.0000
y	0.0000	0.0000	0.0000	0.0000	0.0000
z	0.0000	0.0000	0.0000	0.0000	0.0000
Occupancy	0.1204	0.1208	0.1208	0.1390	0.1408
O					
x	0.5000	0.5000	0.5000	0.5000	0.5000
y	0.5000	0.5000	0.5000	0.5000	0.5000
z	0.5000	0.5000	0.5000	0.5000	0.5000
Occupancy	0.9994	0.9994	1.0069	1.0290	0.9986
R_P	4.21	2.71	1.79	1.51	1.99
R_{WP}	6.15	2.82	2.25	1.90	2.55
R_{Exp}	10.5	3.25	3.12	2.34	3.12
χ^2	0.346	0.45	0.56	0.62	0.58
R_{Bragg}	8.27	2.65	3.15	1.06	8.3
R_F	4.27	1.44	2.14	0.642	4.9
X-ray density (g/cc^3)	6.402	6.418	7.453	7.876	7.183

TABLE 3: SAED (TEM) Parameters of MgO NPs.

Spot#	D -Spacing (nm)	Rec. Pos.(1/nm)	Degrees to Spot 1	Degrees to x-axis	Amplitude
1	0.2324	4.302	0.00	98.98	7845.52
2	0.1639	6.102	7.44	91.54	4185.33
3	0.1328	7.529	5.23	93.75	2049.97
4	0.1156	8.652	2.19	101.17	1236.80
5	0.1031	9.703	9.83	89.15	1214.00

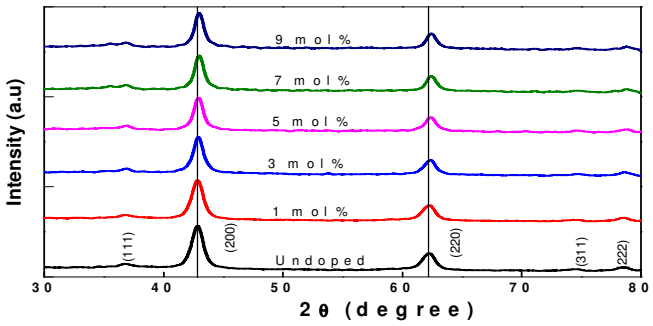

Fig. 1. PXRD patterns of undoped and trivalent Tb -doped MgO.

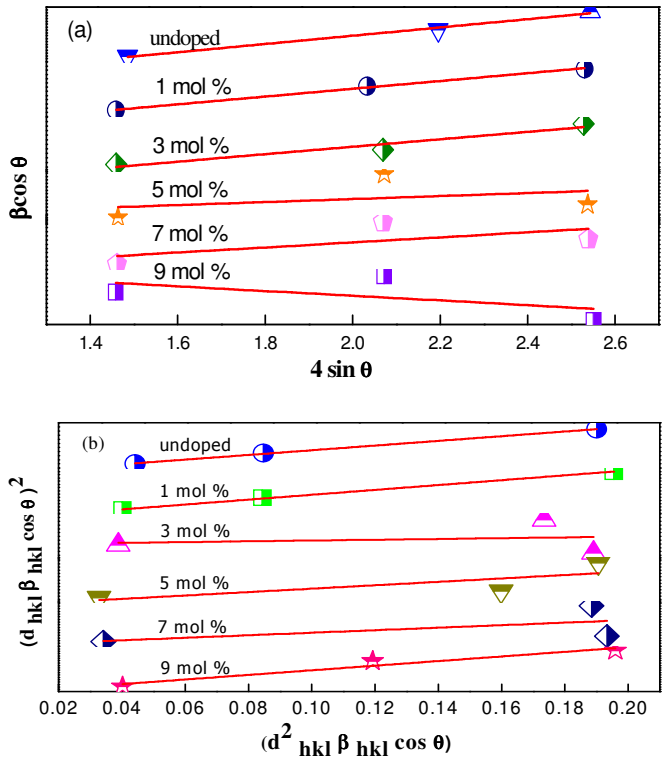

Fig. 2. (a) W-H plots of trivalent Tb doped MgO (1-9 mol%). (b) Strain-Size plots of trivalent Tb doped MgO (1-9 mol%).

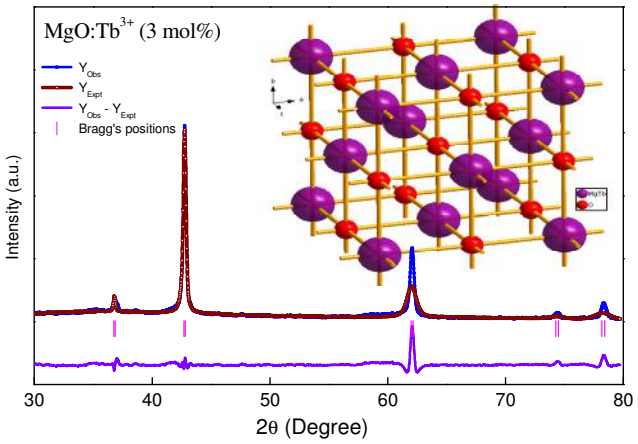

Fig. 3. Rietveld refinement for trivalent Tb doped MgO (3 mol%) nanophosphor.

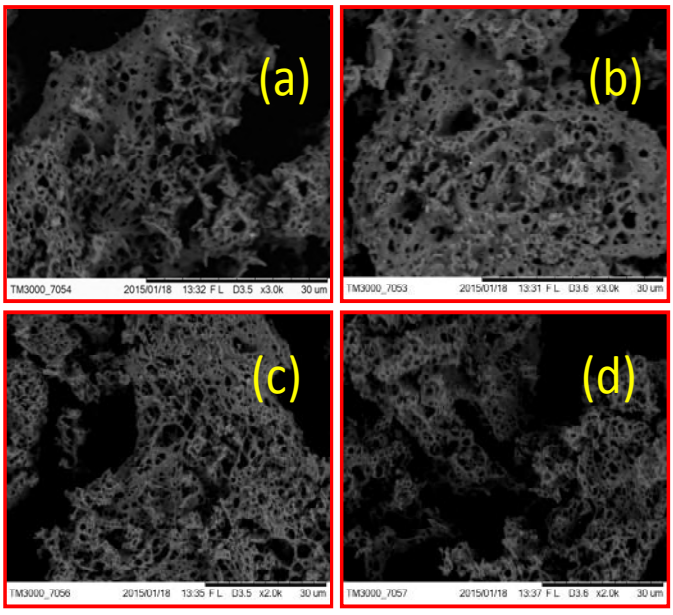

Fig. 4. SEM images A) undoped B) 1 C) 5 D) 9 mol % trivalent Tb doped MgO.

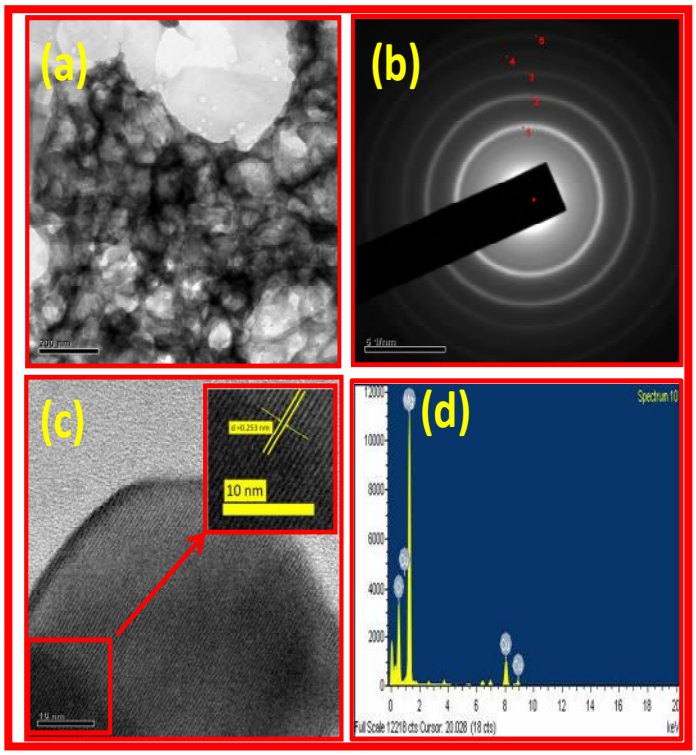

Fig. 5. TEM, SAED, HRTEM and EDAX pattern of pristine MgO.

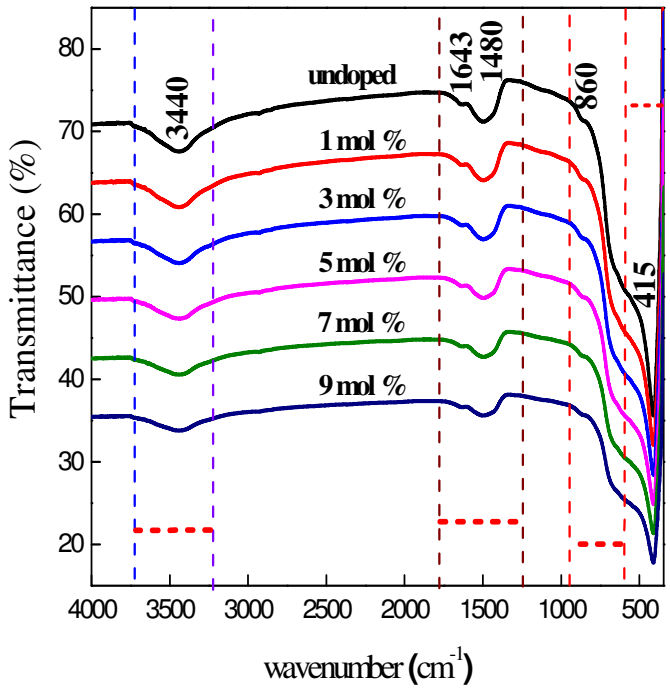

Fig. 6. FT-IR signature of undoped and (1-9 mol%) trivalent Tb doped MgO.

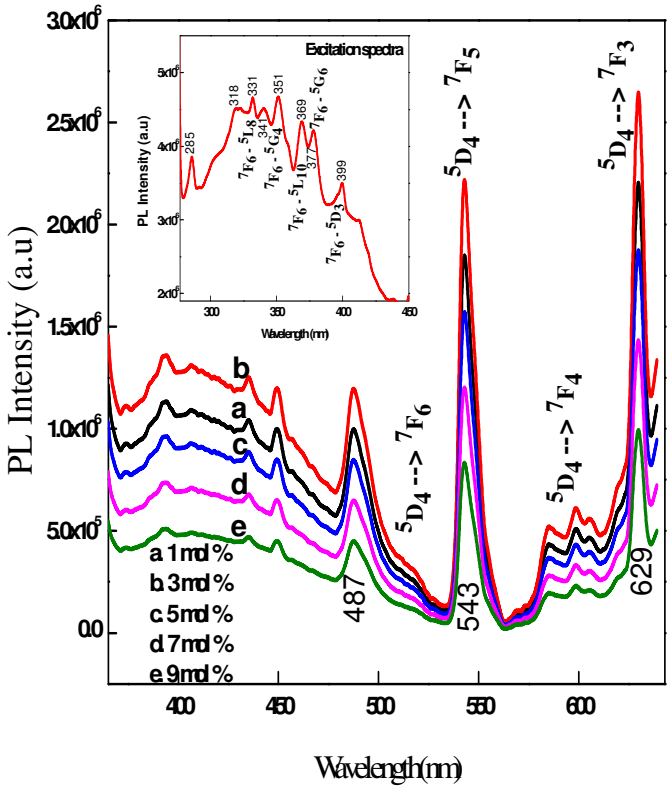

Fig. 7.Emission spectra of MgO: Tb^{3+} (1-9 mol %) (Inset: Excitation spectra of 3 mol % MgO:Tb^{3+}, λ_{emi}=544 nm).

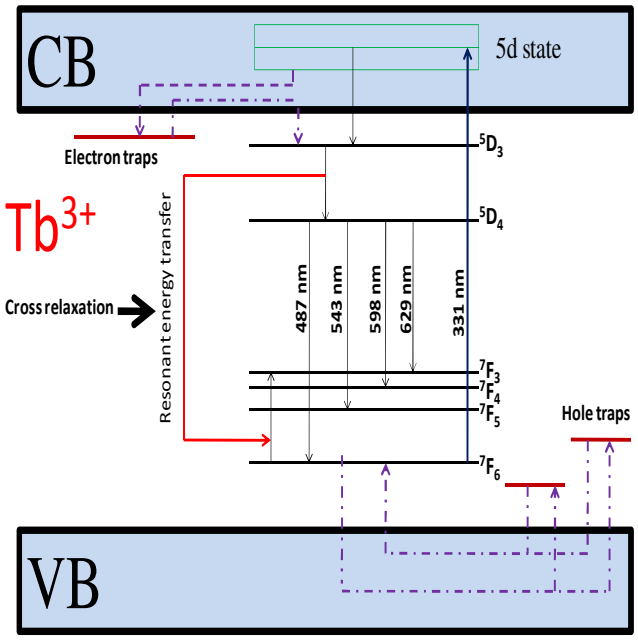

Fig. 8. Emission probabilities of trivalent Tb doped MgO pristine shown by energy level diagram.

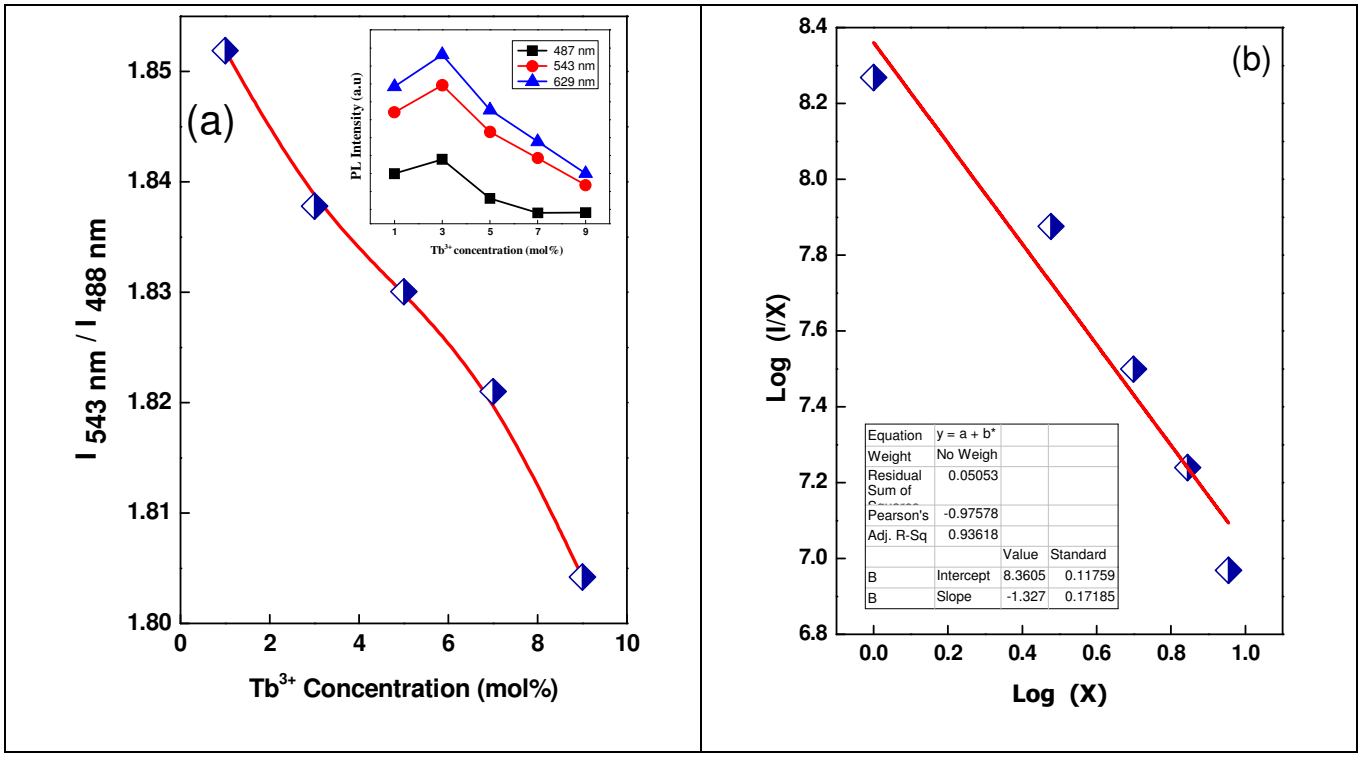

Fig. 9. (a) The effect of Tb^{3+} on the 543 nm emission peak and variation of asymmetric ratio with Tb^{3+} concentration (Inset: Variation of PL Intensity with different mol concentration of Tb^{3+}) (b) Relation between log(x) and log (I/x) in MgO: Tb^{3+} (1-9 mol %) nanophosphors.

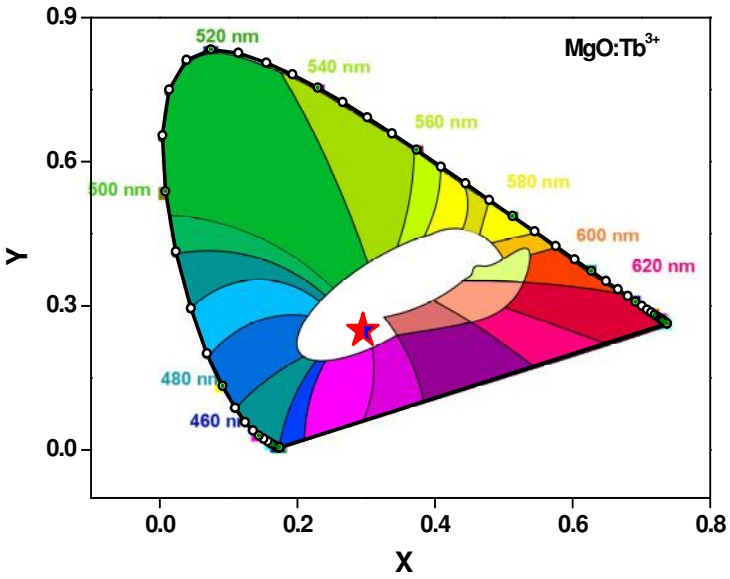

Fig. 10. CIE diagram of MgO: Tb^{3+} (3 mol %). [Inset (x,y) co-ordinate values of 3 mol % MgO:Tb^{3+}].

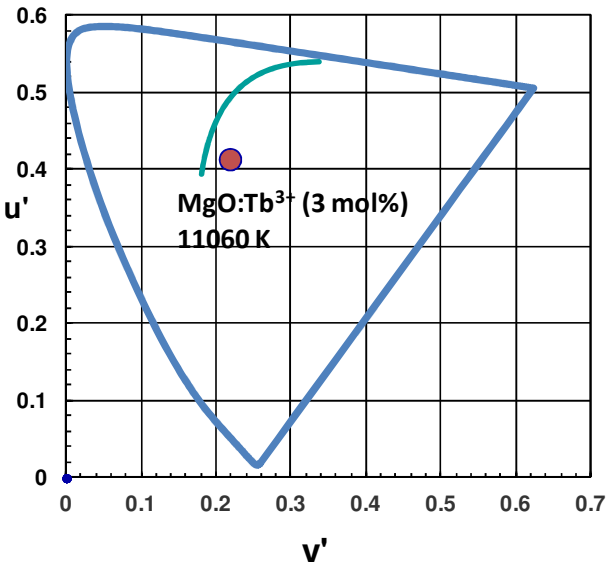

Fig. 11. CCT diagram of MgO:Tb^{3+} (3 mol %) nanophosphor